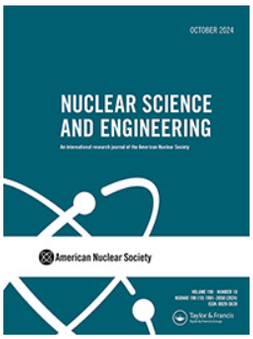

Nuclear Science and Engineering

ISSN: (Print) (Online) Journal homepage: www.tandfonline.com/journals/unse20

A General Formulation of the Resonance Spectrum Expansion Self-Shielding Method

Alain Hébert

To cite this article: Alain Hébert (12 Aug 2024): A General Formulation of the Resonance Spectrum Expansion Self-Shielding Method, Nuclear Science and Engineering, DOI: 10.1080/00295639.2024.2375908

To link to this article: https://doi.org/10.1080/00295639.2024.2375908

NUCLEAR SCIENCE AND ENGINEERING

DOI: https://doi.org/10.1080/00295639.2024.2375908

A General Formulation of the Resonance Spectrum Expansion Self-Shielding Method

Alain Hébert*

Polytechnique Montréal, P.O. Box 6079, Station Centre-Ville, Montréal, Québec, Canada

Received May 6, 2024
Accepted for Publication June 14, 2024

Abstract — *The resonance spectrum expansion (RSE) self-shielding method was recently proposed by Nagoya and Osaka universities as a powerful alternative to existing approaches. First investigations of the RSE at Polytechnique Montreal show that it can effectively replace the actual subgroup method used for production calculations in DRAGON5. The Japanese implementation of the RSE method is limited to a solution of the Boltzmann transport equation (BTE) with the method of characteristics. We are proposing a new implementation of the RSE method compatible with various types of solutions for the BTE, including the collision probability and the interface current methods. We based our validation study on a subset made up of eight Rowlands pin cell benchmark cases. The absorption rates obtained after self-shielding are compared with exact values obtained using an elastic slowing-down calculation where each resonance is modeled individually in the resolved energy domain. Validation of Rowlands benchmark with effective multiplication factor calculations was also conducted with respect of the SERPENT2 Monte Carlo code. It is shown that the RSE method is compatible with both advanced and legacy energy meshes and performs slightly better than the production subgroup methods actually used.*

Keywords — *Lattice calculation, resonance self-shielding, resonance spectrum expansion, reduced-order model, proper orthogonal decomposition.*

Note — *Some figures may be in color only in the electronic version.*

I. INTRODUCTION

The purpose of the resonance self-shielding calculations in a lattice code is to produce averaged microscopic cross sections over coarse energy groups to be used later in a solution of the Boltzmann transport equation (BTE).[1] These calculations are based on different approximations. The state-of-the-art approach relies on the subgroup (or multiband) approach in which the detailed energy-dependent cross-section behavior in each coarse energy group is replaced by its probability density representation.[2,3] An accurate discretization of each probability density is then obtained, leading to quadrature sets called probability tables.

These probability tables are subsequently used within the flux solution algorithm of the subgroup method. The subgroup projection method (SPM) is a recent implementation of the subgroup method available in the DRAGON5 lattice code.[4,5] Such method is considered the state of the art for the generation of self-shielded cross sections for pressurized water reactor assemblies.

The resonance spectrum expansion (RSE) method was recently proposed as an alternative to existing subgroup

*E-mail: alain.hebert@polymtl.ca

methods.[6,7] The RSE method is based on a reduced-order model in which the resonant flux in each coarse energy group is expanded as a linear combination of snapshot functions. A reduced set of basis functions are obtained through a proper orthogonal decomposition (POD) technique so that they can reproduce the actual resonant flux with a relatively small number of degrees of freedom. This number of degrees of freedom is the POD rank and is equal to or smaller than the number of snapshot functions. These snapshot functions are related to solutions of the NJOY flux calculator for a list of dilutions.[8]

The RSE formulations proposed in Refs. [6,7] are limited to solutions of the neutron fluxes with the method of characteristics (MOC), an expensive class of solutions for the BTE, particularly for self-shielding uses. Here, we propose a modified RSE approach based on linear transformations that are compatible with simplified solutions of the BTE, in particular those based on the collision probability or on the interface current methods.

In this paper, we show that the RSE method can be reformulated as an improved subgroup method with better mathematical foundations than the existing approaches. The proposed implementation is a modification of the SPM, as described in Ref. [9], and is available in the lattice code DRAGON5. Section II is discusses the adaptation of DRAGON5 for cases where each resonant isotope is self-shielded independently without taking into account mutual resonance shielding effects. The existing SPM correlation model for representing mutual resonance shielding effects is available now, although it is not validated in this paper.

II. THEORY

A few assumptions have been made for the heavy slowing-down operator $R^*\{\varphi(\boldsymbol{r},u)\}$ at energies where the resonance self-shielding model is applied. We assume that scattering by the absorber is elastic and isotropic in the center of mass, and that the target nucleus is effectively at rest in the laboratory system. However, the scattering source at lethargy u' will reflect the true material temperature since elastic scattering cross sections are Doppler broadened. This representation is written

$$\frac{1}{N^*}\,R^*\{\varphi(\boldsymbol{r},u)\} = \frac{1}{1-\alpha}\int_{u-\epsilon}^{u} du'\,e^{u'-u}\,\sigma_s^*(\boldsymbol{r},u')\,\varphi(\boldsymbol{r},u') \quad , \tag{1}$$

where N^* is the number density of the resonant isotope, $\varphi(\boldsymbol{r},u)$ is the fine-structure function, and $\sigma_s^*(\boldsymbol{r},u)$ is the microscopic elastic scattering cross section of the resonant isotope. The parameters α and ϵ are defined as a function of the mass ratio A as

$$\alpha = \left(\frac{A-1}{A+1}\right)^2 \quad \text{and} \quad \epsilon = \ln\frac{1}{\alpha} \quad . \tag{2}$$

The Livolant-Jeanpierre [Eq. (4-37) introduced in Sec. 4.2.3 of Ref. [1]] is a simplified transport equation that can be used to describe a heterogeneous case with a unique or mixture of resonant isotopes. Here, we consider its solution over a coarse group g where the nonresonant cross sections are assumed to be constant in lethargy. We write

$$\begin{aligned}&\boldsymbol{\Omega}\cdot\nabla\varphi(\boldsymbol{r},u,\boldsymbol{\Omega}) + \Sigma(\boldsymbol{r},u)\varphi(\boldsymbol{r},u,\boldsymbol{\Omega})\\ &\quad = \frac{1}{4}\pi\left[\Sigma_{s,g}^{+}(\boldsymbol{r}) + R^*\{\varphi(\boldsymbol{r},u)\}\right] \quad ,\end{aligned} \tag{3}$$

where $\Sigma(\boldsymbol{r},u)$ is the macroscopic total cross section and $\Sigma_{s,g}^{+}(\boldsymbol{r})$ is the macroscopic scattering cross section of the nonresonant isotopes at position $\boldsymbol{r}$ in coarse group g. The assumption of isotropic source is justified since anisotropic contributions have a negligible impact on resonance self-shielding.[6] The fine-structure function $\varphi(\boldsymbol{r},u,\boldsymbol{\Omega})$ is a generalization to the heterogeneous case for the solution of the flux calculator in module groupr of NJOY.[8]

The NJOY flux calculator equation is written

$$\left[\sigma_{e,g} + \sigma^*(u)\right]\varphi(u) = \sigma_{e,g} + \frac{1}{N^*}R^*\{\varphi(u)\} \quad , \tag{4}$$

where $\sigma^*(u)$ is the microscopic total cross section of the resonant isotope and where the dilution of the resonant isotope in the infinite homogeneous medium is defined as

$$\sigma_{e,g} = \frac{\Sigma_g^{+}}{N^*} \quad , \tag{5}$$

where Σ_g^{+} is the macroscopic total cross section of the nonresonant isotopes.

Equation (4) is the infinite homogeneous version of Eq. (3). NJOY provides solutions of Eq. (4) using a continuous-energy representation of cross sections. Solutions are obtained for a list of dilutions $\sigma_{e,g}$ (including infinite dilution $\sigma_{e,g} = 1.0\times10^{10}$ b) and a list of absolute temperatures.

II.A. Resonance Spectrum Expansion

An Autolib lethargy mesh, also known as an ultra-fine group (UFG) mesh, is defined in each coarse group g

so as to describe precisely each resonance of the resolved energy domain.[10] The width of each element of the UFG mesh is an integer multiple of an elementary width Δu_{elem}. The RSE treatment starts by temperature interpolation of information available in the multigroup cross-section library of the lattice code and recovered from NJOY. The DRAGON family of lattice codes use multigroup cross-section libraries in the DRAGLIB format containing the suitable information. They are produced by the dragr module of NJOY.[11] This information includes the following:

1. *Total and scattering microscopic cross sections defined over the Autolib mesh*. These are arrays of size $N_{\text{ufg},g}$, the number of UFGs in coarse group g.

2. *Matrices $\mathbb{X}_g$ of size $N_{\text{part}} \times N_{\text{dil}}$ containing information integrated over coarse groups*. N_{part} is one plus the number of cross-section types, and N_{dil} is the number of dilutions. Cross-section types are the total, diffusion, and additional types, such as ν-fission, diffusion for all Legendre orders, scattering for all Legendre orders and all secondary coarse groups, delayed fission, and other selected types in NJOY [(n, *x*n), etc.]. Each line of $\mathbb{X}_g$ contains values of one of these three types:

   a. averaged UFG fine-structure function in coarse group g,

$$< \varphi >_g = \frac{1}{u_g - u_{g-1}} \int_{u_{g-1}}^{u_g} du\, a\, \varphi(u) \tag{6}$$

   b. averaged effective total rate in coarse group g,

$$< \sigma^* \varphi >_g = \frac{1}{u_g - u_{g-1}} \int_{u_{g-1}}^{u_g} du\, a\, \sigma^*(u)\varphi(u) \tag{7}$$

   c. averaged effective partial rate for partial reaction ρ in coarse group g,

$$< \sigma^*_\rho \varphi >_g = \frac{1}{u_g - u_{g-1}} \int_{u_{g-1}}^{u_g} du\, a\, \sigma^*_\rho(u)\varphi(u) \quad . \tag{8}$$

We also need to define a UFG cross-section matrix $\mathbb{Q}_g$ of size $N_{\text{part}} \times N_{\text{ufg},g}$ in each coarse group. The first line of $\mathbb{Q}_g$ is a row vector of ones, and the second and third lines of $\mathbb{Q}_g$ contain the microscopic total and P_0 diffusion cross sections recovered from the Autolib. Subsequent lines contain additional cross-section types not available in the Autolib. Matrix $\mathbb{Q}_g$ is used in the theoretical derivation of the probability tables, but is not used in its computer implementation.

Equation (4) is solved in the lattice code over the UFG mesh for the same list of dilutions $\sigma_{e,g}$ previously used in NJOY. Snapshot matrices $\mathbb{A}_g$ of size $N_{\text{ufg},g} \times N_{\text{dil}}$ are set where each column of $\mathbb{A}_g$ is the UFG solution of Eq. (4) for a specific dilution, namely, $\varphi_g^{(m)} \Delta u_g^{(m)}, m \leq N_{\text{ufg},g}$, where $\Delta u_g^{(m)}$ is a UFG lethargy width.

The continuous-energy solution from NJOY is not available in the lattice code. However, we have access to the integrated fine-structure functions from NJOY. There is a tiny discrepancy between the values recovered from NJOY and those obtained from the UFG solution of the lattice code. This discrepancy is taken into account by the normalization of the $\mathbb{A}_g$ snapshot matrices in such a way that the snapshot fine-structure functions integrated over a coarse group are equal to the values computed in NJOY.

Using the previous definition, we can write a relation between the following matrices as

$$\mathbb{X}_g = \frac{1}{u_g - u_{g-1}} \mathbb{Q}_g \mathbb{A}_g \quad . \tag{9}$$

The RSE information is obtained from the Autolib data using a singular value decomposition (SVD) of the form

$$\mathbb{A}_g = \mathbb{U}_g \mathbb{W}_g \mathbb{V}_g^{\mathrm{T}} \quad , \tag{10}$$

where $\mathbb{U}_g$ is the first orthogonal SVD matrix of size $N_{\text{ufg},g} \times K_g$, $\mathbb{W}_g$ is the singular-value diagonal matrix of size $K_g \times K_g$, $\mathbb{V}_g$ is the second orthogonal SVD matrix of size $N_{\text{dil}} \times K_g$, and where K_g is the POD rank in coarse group g.

The singular values in matrix $\mathbb{W}_g$ appear with decreasing magnitude. The K_g maximum singular values, those $> \epsilon_{\text{svd}} \Delta u_{\text{elem}}$, are kept in the RSE algorithm. Here, Δu_{elem} is the elementary lethargy width of the Autolib. A value of $\epsilon_{\text{svd}} = 1.0 \times 10^{-3}$ is set by default, but can be redefined by the user. Using a coarser value leads to shorter CPU times for both generations of probability tables and for solving the resulting subgroup equations. The SVD algorithm is powerful at eliminating basis redundancies so that $K_g \leq N_{\text{dil}}$.

The columns of the $\mathbb{U}_g$ matrix are used as basis functions by the RSE method. The RSE fine-structure function expansion in UFG m is written as

$$\varphi_g^{(m)}(\boldsymbol{r},\,\boldsymbol{\Omega}) = \frac{1}{\Delta u_g^{(m)}} \sum_{k=1}^{K_g} \psi_k(\boldsymbol{r},\,\boldsymbol{\Omega}) U_{m,k} \quad , \tag{11}$$

where $U_{m,k}$ is an element of $\mathbb{U}_g$ and $\psi_k(\boldsymbol{r},\,\boldsymbol{\Omega})$ is the expansion coefficient. This basis is orthonormal, as

$$\sum_{m=1}^{N_{\mathrm{ufg},g}} U_{m,k} U_{m,\ell} = \delta_{k,\ell} \quad . \tag{12}$$

Equation (11) is the principal approximation of the RSE method in the case where the resonant isotope is unique.

Equation (3) is first discretized over the UFG mesh, leading to the Autosecol fine structure equation,

$$\boldsymbol{\Omega} \cdot \nabla \varphi_g^{(m)}(\boldsymbol{r},\,\boldsymbol{\Omega}) + \Sigma_g^{(m)}(\boldsymbol{r}) \varphi_g^{(m)}(\boldsymbol{r},\,\boldsymbol{\Omega})$$

$$= \frac{1}{4\pi} \left[\Sigma_{\mathrm{s},g}^{+}(\boldsymbol{r}) + N^*(\boldsymbol{r}) \sum_{h=1}^{g} \sum_{n=1}^{N_{\mathrm{ufg},h}} \sigma_{\mathrm{s},g\leftarrow h}^{*(m\leftarrow n)} \varphi_h^{(n)}(\boldsymbol{r}) \frac{\Delta u_h^{(n)}}{\Delta u_g^{(m)}} \right] \quad . \tag{13}$$

We next substitute Eq. (11) into Eq. (13) and obtain its moments with the application of a weight-residual approach. We obtain a coarse-group formulation of the Livolant-Jeanpierre equation as

$$\begin{aligned} &\boldsymbol{\Omega} \cdot \nabla \psi_{k,g}(\boldsymbol{r},\,\boldsymbol{\Omega}) + \Sigma_g^{+}(\boldsymbol{r}) \psi_{k,g}(\boldsymbol{r},\,\boldsymbol{\Omega}) \\ &+ N^*(\boldsymbol{r}) \sum_{\ell=1}^{K_g} \widetilde{\sigma}_{k,\ell,g}^{*} \psi_{\ell,g}(\boldsymbol{r},\,\boldsymbol{\Omega}) \\ &= \frac{1}{4\pi} \left[\widetilde{\gamma}_{k,g} \Sigma_{\mathrm{s},g}^{+}(\boldsymbol{r}) + N^*(\boldsymbol{r}) \sum_{h=1}^{g} \sum_{\ell=1}^{K_h} \widetilde{\sigma}_{\mathrm{s},k,\ell,g\leftarrow h}^{*} \psi_{\ell,h}(\boldsymbol{r}) \right] \quad , \end{aligned} \tag{14}$$

where $g = 1, G$, $k = 1, K_g$, and where

$$\widetilde{\sigma}_{k,\ell,g}^{*} = \sum_{m=1}^{N_{\mathrm{ufg},g}} U_{m,k} U_{m,\ell} \sigma_g^{*(m)} \quad , \tag{15}$$

$$\widetilde{\sigma}_{\mathrm{s},k,\ell,g\leftarrow h}^{*} = \sum_{m=1}^{N_{\mathrm{ufg},g}} \sum_{n=1}^{N_{\mathrm{ufg},h}} U_{m,k} U_{n,\ell} \sigma_{\mathrm{s},g\leftarrow h}^{*(m\leftarrow n)} \quad , \tag{16}$$

and

$$\widetilde{\gamma}_{k,g} = \sum_{m=1}^{N_{\mathrm{ufg},g}} \Delta u_g^{(m)} U_{m,k} \quad , \tag{17}$$

where $\sigma_g^{*(m)}$ and $\sigma_{\mathrm{s},g\leftarrow h}^{*(m\leftarrow n)}$ are the UFG total and scattering resonant microscopic cross sections, respectively.

Another useful quantity, $\widetilde{\omega}_{k,g}$, is defined as

$$\widetilde{\omega}_{k,g} = \frac{1}{u_g - u_{g-1}} \sum_{m=1}^{N_{\mathrm{ufg},g}} U_{m,k}. \tag{18}$$

Equation (14) was first obtained as Eq. (12) in Ref. [6]. Unfortunately, it is not equivalent to a subgroup equation due to the sum over K_g in the left side. However, the summation over K_h in the right side has been previously proposed in Ref. [12] in the context of an improved subgroup approximation. Similarly, the summation over groups $\leq h$ in the right side has been previously proposed in Ref. [13] as the *toutes résonances* model of the fine-structure self-shielding method and implemented in the APOLLO2 lattice code. Equation (14) must be solved using a dedicated method, such as the modified MOC proposed in Ref. [6] or Ref. [7]. The modified MOC is based on matrix exponential terms obtained via the Cayley-Hamilton theorem.

The main motivation for using subgroup equations is their compatibility with existing or legacy numerical techniques of BTE solutions, such as the collision probability or the interface current methods. In this paper, we propose an alternative approach, based on a linear transformation of Eq. (14), so as to obtain a subgroup compatible equation. Moreover, we propose the weighting of matrix $\mathbb{X}_g$ so as to obtain a probability table compatible with the RSE method. Such probability tables are consistent: The base points $\sigma_{k,g}^{*}$ are constrained as $\min(\sigma^*(u)) \leq \sigma_{k,g}^{*} \leq \max(\sigma^*(u))$ in coarse group g, the values of the probability table are real, and the weights are positive.

The next step consists of writing $\widetilde{\sigma}_{k,\ell,g}^{*}$ as a $\mathbb{S}_g$ matrix of size $K_g \times K_g$ and finding all its eigenvectors $\boldsymbol{t}_{k,g}$ with the associated eigenvalues $\sigma_{k,g}^{*}$. These eigenvalues are the base points of the proposed subgroup formulation. They are real because the $\mathbb{S}_g$ matrix is symmetric. We build a matrix $\mathbb{T}_g$ whose columns are the eigenvectors of $\mathbb{S}_g$. This matrix is written as

$$\mathbb{T}_g = [\boldsymbol{t}_{1,g}\ \ \boldsymbol{t}_{2,g}\ \ \ldots\ \ \boldsymbol{t}_{K,g}] \tag{19}$$

so that

$$\mathbb{S}_g\mathbb{T}_g = \mathbb{T}_g\left[\mathrm{diag}(\sigma^*_{k,g})\right] \quad . \tag{20}$$

The linear transformation technique used to rewrite Eq. (14) is based on the introduction of the unknown vector $\boldsymbol{\zeta}_g(\boldsymbol{r},\ \boldsymbol{\Omega}) = \mathrm{col}[\zeta_{1,g}(\boldsymbol{r},\ \boldsymbol{\Omega})\ \zeta_{2,g}(\boldsymbol{r},\ \boldsymbol{\Omega})\ \ldots\ \zeta_{K,g}(\boldsymbol{r},\ \boldsymbol{\Omega})]$ defined in such a way that

$$\boldsymbol{\Psi}_g(\boldsymbol{r},\ \boldsymbol{\Omega}) = \mathbb{T}_g\ \boldsymbol{\zeta}_g(\boldsymbol{r},\ \boldsymbol{\Omega}) = \begin{bmatrix} t_{11,g} & t_{12,g} & \ldots & t_{1K,g} \\ t_{21,g} & t_{22,g} & \ldots & t_{2K,g} \\ \vdots & \vdots & \ddots & \vdots \\ t_{K1,g} & t_{K2,g} & \ldots & t_{KK,g} \end{bmatrix} \begin{bmatrix} \zeta_{1,g}(\boldsymbol{r},\ \boldsymbol{\Omega}) \\ \zeta_{2,g}(\boldsymbol{r},\ \boldsymbol{\Omega}) \\ \vdots \\ \zeta_{K,g}(\boldsymbol{r},\ \boldsymbol{\Omega}) \end{bmatrix} \quad . \tag{21}$$

The substitution of Eq. (21) into Eq. (14) and the left-multiplication of both the left side and the right side terms by $\mathbb{T}_g^{\mathrm{T}}$ leads to

$$\boldsymbol{\Omega}\cdot\nabla\zeta_{k,g}(\boldsymbol{r},\boldsymbol{\Omega}) + \left[\Sigma_g^+(\boldsymbol{r}) + N^*(\boldsymbol{r})\sigma^*_{k,g}\right]\zeta_{k,g}(\boldsymbol{r},\ \boldsymbol{\Omega}) = \frac{1}{4\pi}\left[\gamma_{k,g}\Sigma^+_{\mathrm{s},g}(\boldsymbol{r}) + N^*(\boldsymbol{r})\sum_{h=1}^{G}\sum_{\ell=1}^{K_h}\sigma^*_{\mathrm{s},k,\ell,g\leftarrow h}\zeta_{\ell,h}(\boldsymbol{r})\right] , \tag{22}$$

where $g = 1, G$; $k = 1, K_g$; and where the scattering and gamma terms are obtained as

$$\left[\sigma^*_{\mathrm{s}}\right]_{g\leftarrow h} = \mathbb{T}_g^{\mathrm{T}}\left[\widetilde{\sigma}^*_{\mathrm{s}}\right]_{g\leftarrow h}\mathbb{T}_h \ , \tag{23}$$

$$\boldsymbol{\gamma}_g = \mathbb{T}_g^{\mathrm{T}}\widetilde{\boldsymbol{\gamma}}_g \ . \tag{24}$$

and

$$(\boldsymbol{\omega})_g = \mathbb{T}_g^{\top}(\widetilde{\boldsymbol{\omega}})_g. \tag{25}$$

The components $\gamma_{k,g}$ are proportional to the infinite-dilution unknowns $\zeta_{k,g}(\boldsymbol{r},\ \boldsymbol{\Omega})$. Equation (22) is a subgroup equation similar to Eq. (4.76) in Ref. [1]. A consequence of this linear transformation is the possibility to adapt the RSE method to a subgroup implementation similar to those one available in the USS: module of DRAGON5.[5] Equation (22) is solved iteratively to obtain the K_g solution vectors, starting from an initial estimate equal to $\boldsymbol{\gamma}_{\mathbf{g}}$. At any time during the iterations, the averaged UFG fine-structure function $<\varphi(\boldsymbol{r})>_g$ and the effective rates $<\sigma^*_{\rho}\varphi((r))>_g$ can be obtained as

$$<\varphi((\boldsymbol{r}))>_g = (\boldsymbol{\omega})_g^{\top}(\boldsymbol{\zeta})_g((\boldsymbol{r})) \tag{26}$$

and

$$<\sigma^*_{\rho}\varphi((\boldsymbol{r}))>_{\boldsymbol{g}} = (\boldsymbol{\omega})_g^{\top}\left[\mathrm{diag}(\sigma^*_{\rho,k,g})\right](\boldsymbol{\zeta})_g((\boldsymbol{r})). \tag{27}$$

Effective rates for reaction ρ can be written in the term of Riemann integrals or Lebesgue quadratures as

$$<\sigma^*_{\rho}\varphi(\boldsymbol{r})>_g = \frac{1}{u_g - u_{g-1}}\int_{u_{g-1}}^{u_g} du\sigma^*_{\rho}(u)\varphi(u) = \sum_{k=1}^{K_g}\omega_{k,g}\sigma^*_{\rho,k,g}\zeta_{k,g}(\boldsymbol{r}) \ . \tag{28}$$

A probability table matrix $\mathbb{P}_g$, of size $N_{\mathrm{part}}\times K_g$ and correlated with the base points $\sigma^*_{k,g}$, is defined as

$$\mathbb{P}_g = \begin{bmatrix} \omega_{1,g} & \omega_{2,g} & \ldots & \omega_{K_g,g} \\ \omega_{1,g}\sigma^*_{1,g} & \omega_{2,g}\sigma^*_{2,g} & \ldots & \omega_{K_g,g}\sigma^*_{K_g,g} \\ \omega_{1,g}\sigma^*_{\rho,1,g} & \omega_{2,g}\sigma^*_{\rho,2,g} & \ldots & \omega_{K_g,g}\sigma^*_{\rho,K_g,g} \end{bmatrix} , \tag{29}$$

where the $\sigma^*_{\rho,k,g}$ terms are representing $N_{\mathrm{part}}-2$ components each. Equation (28) is satisfied in each coarse group g if

$$\frac{1}{u_g - u_{g-1}}\mathbb{Q}_g\mathrm{col}\left[\Delta u_g\varphi_g(\boldsymbol{r})\right] = \mathbb{P}_g\boldsymbol{\zeta}_g(\boldsymbol{r}) \ , \tag{30}$$

where $\mathrm{col}\left[\Delta u_g\varphi_g(\boldsymbol{r})\right]$ and $\boldsymbol{\zeta}_g(\boldsymbol{r})$ are column vectors of size $N_{\mathrm{ufg},g}$ and K_g, respectively.

Using Eqs. (11) and (21), Eq. (30) can be rewritten as

$$\frac{1}{u_g - u_{g-1}}\mathbb{Q}_g\mathbb{U}_g\mathbb{T}_g\ \boldsymbol{\zeta}_{\mathbf{g}}(\boldsymbol{r}) = \mathbb{P}_g\boldsymbol{\zeta}_{\mathbf{g}}(\boldsymbol{r}) \tag{31}$$

so that

$$\mathbb{P}_g = \frac{1}{u_g - u_{g-1}}\mathbb{Q}_g\mathbb{U}_g\mathbb{T}_g \ . \tag{32}$$

Equation (32) cannot be used directly because matrix $\mathbb{Q}_g$ is unknown. We need to rewrite Eq. (32) with the help of Eqs. (9) and (10) so that it can be computed with the available information,

$$\mathbb{P}_g = \frac{1}{u_g - u_{g-1}} \mathbb{Q}_g \left[\mathbb{A}_g \mathbb{V}_g \mathbb{W}_g^{-1} \right] \mathbb{T}_g = \mathbb{X}_g \mathbb{V}_g \mathbb{W}_g^{-1} \mathbb{T}_g \ . \quad (33)$$

The RSE-based probability tables, including correlation information, are computed for each distinct resonant isotope and are independent of its number density. We currently do not support the production of probability tables for a mixture of many resonant isotopes, as proposed in the original RSE method of Ref. [6]. We never solve Eq. (4) for a mixture of isotopes. What we do is solve Eq. (4) for a distinct resonant isotope and perform subgroup projections for other resonant isotopes on the resonant isotope being processed.

The process of computing probability tables is more time consuming with the RSE method than it is with the CALENDF tables. This information is computed once in homogeneous geometry condition before the burnup loop, and remains valid as long as the nuclide temperature does not change. The subgroup Eq. (22) is solved repeatedly in heterogeneous geometry condition during the burnup loop, using known probability tables. In real production cases, the subgroup solution represents the largest part of CPU resources. This is not the case with the Rowlands benchmarks in Sec. III, which are too simple to provide meaningful CPU time values.

The RSE method can only be implemented in the resolved energy domain where the Autolib data are available. We propose using physical probability tables in the unresolved energy domain, as proposed in Sec. 4.2.4 of Ref. [1]. The following simplified subgroup equation was therefore used in the unresolved energy domain:

$$\boldsymbol{\Omega} \cdot \nabla \psi_{k,g}(\boldsymbol{r}, \boldsymbol{\Omega}) + \left[\Sigma_g^+(\boldsymbol{r}) + N^*(\boldsymbol{r}) \sigma_{k,g}^* \right] \psi_{k,g}(\boldsymbol{r}, \boldsymbol{\Omega}) = \frac{1}{4\pi} \left[\Sigma_{s,g}^+(\boldsymbol{r}) + N^*(\boldsymbol{r}) \sum_{\ell=1}^{K_g} \omega_{\ell,g} \sigma_{s,\ell,g}^* \psi_{\ell,g}((r)) \right] , \quad (34)$$

where $g = 1, G$ and $k = 1, K_g$.

III. NUMERICAL RESULTS

We based our validation study on a subset made up of eight Rowlands pin cell benchmark cases[14] with the SPM. Uranium-oxide (UOX) and mixed-oxide (MOX) calculations use a SHEM-295 JEFF 3.1.1–based library built from scratch with NJOY[8] release 2012.139, including the dragr module. A NJOY-2016 implementation is also available.[11] Draglib data include temperature-dependent Autolib data for all resonant isotopes between 22.54 eV and 11.14 keV for the SHEM-281 library (corresponding to $93 \geq g \geq 56$) and between 4.63 eV and 11.14 keV for the SHEM-295 library (corresponding to $206 \geq g \geq 56$).[4,15]

The elementary lethargy width of the Autolib data is 5×10^{-4} up to 100 eV and 1.25×10^{-4} at higher energies. The resolved energy domain of the 281g and 295g energy meshes are represented with 40,183 and 43,812 UFG energy bins, respectively. The dilution grid is user selected in NJOY and can be different from one isotope to the other. By default, infinite dilution and 18 finite dilution values are selected between 1.5 and 10000.0 b, equally spaced on a logarithmic mesh. This represents 19 snapshots with potential degeneracy for some of them. For example, the 10000.0 b snapshot can be almost identical to the infinite dilution one. However, the POD technique is efficient at removing any snapshot degeneracy. Three types of probability tables were used in this study:

1. *SUBG*: Physical probability tables as described in Secs. 4.2.4 and 4.2.5 of Ref. [1]. These tables are adapted to the SHEM-281 library.

2. *CALENDF*: Mathematical probability tables as described in Ref. [4]. These tables are adapted to the SHEM-295 library.

3. *RSE*: Probability tables as described in this paper. These tables are adapted to both libraries.

All DRAGON5 calculations are based on the SYBILT: tracking module applied to a square pin cell and implementing a collision probability solution. The fuel rod is submeshed into subvolume fractions of 40%, 30%, 10%, 10%, 5%, and 5% for the outer ring. The self-shielding calculation in DRAGON5 uses SYBILT: tracking with parameters QUA2 20 3 DP01 and the main flux calculation uses SALT: tracking with tracking parameters TSPC EQW2 12 20.0. In all cases, resonance self-shielding models are applied below 11.1 keV (using option GRMIN 56), corresponding to the upper limit of the Autolib mesh.

Comparisons were made for light water reactor square pin cells without leakage. Two types of cells were studied, one UO_2 fueled (UOX), and the other $UPuO_2$ fueled, the latter of which was in two versions with different isotopic compositions (MOX-1 and MOX-2). The calculation of the RSE-based probability tables was activated with keyword in RSE in module LIB: of DRAGON5. This calculation is more CPU intensive than before, but is independent of fuel burnup, fuel density, and the geometry complexity. Most CPU time is spent on the SVDs of Eq. (10) and the eigenvalue solutions of Eq. (20).

III.A. One-Neutron Source Rowlands Benchmark

The absorption rates obtained using the SPM were compared to reference results obtained with the CESCOL UFG method.[4] We shifted the benchmark temperatures from 300 K to 294 K and from 600 K to 550 K in order to avoid temperature interpolation discrepancies. The corresponding numerical results are presented in Tables I through IV for each SHEM mesh and each UOX and MOX benchmark case.

We are reporting global values for maximum ϵ^{max}, averaged $\bar{\epsilon}$, and integrated error ϵ^{int}, corresponding to global, isotopic, and spatially dependent absorption rates. The percent errors in the absorption rates are plotted in Figs. 1 and 2, corresponding to the UOX and MOX first case, respectively. Note that the presence of the 1.0 n/cm^3·s source produces nonphysical transients on absorption rates in group 56. Close inspection of these numerical results leads to the conclusion that the RSE method is slightly more accurate and can effectively replace both the physical probability tables (SUBG option) on coarser energy meshes and the mathematical probability tables (PT option) on the SHEM-295 mesh. The combination of RSE option and SHEM-295 mesh is successful at correcting the absorption rate tilt in the fuel rod.

III.B. Rowlands Benchmark with Effective Multiplication Factor Calculations

The effective multiplication factors obtained for the UOX and MOX cases are shown in Tables V and VI, respectively. Recent ACE files for the JEFF3.1.1 evaluation were processed by the IRSN (Institut de Radioprotection et de Sûreté Nucléaire) and used in this study.[16] Both DRAGON5 and SERPENT2 cross-section libraries are tabulated at the same temperatures. However,

TABLE I

Summary of UOX One-Neutron, 281 g Source Benchmarks with the SPM*

		Case 1 Isothermal 294 K	Case 2 Reduced H_2O Density	Case 3 Fuel at 900 K	Case 4 Isothermal 550 K
SUBG	ϵ^{int} (%)	0.500	0.429	0.571	0.552
	$\bar{\epsilon}$ (%)	0.813	0.840	1.096	1.020
	ϵ^{max} (%)	5.738	5.981	10.501	9.017
	In group	77	77	77	77
	^{235}U ϵ^{int} (%)	−0.221	−0.245	−0.357	−0.296
	^{238}U ϵ^{int} (%)	0.839	0.755	0.967	0.936
	^{238}U ϵ^{int} (%)				
	Ring 1	1.050	1.055	1.355	1.350
	Ring 2	1.521	1.342	1.632	1.559
	Ring 3	2.107	1.941	2.193	2.062
	Ring 4	2.076	1.882	2.456	2.146
	Ring 5	0.387	0.414	0.694	0.599
	Ring 6	−3.855	−4.088	−4.693	−4.318
RSE	ϵ^{int} (%)	0.175	0.196	0.184	0.231
	$\bar{\epsilon}$ (%)	0.850	0.884	1.010	0.992
	ϵ^{max} (%)	5.725	5.991	10.364	8.924
	In group	77	77	77	77
	^{235}U ϵ^{int} (%)	−0.154	−0.190	−0.264	−0.221
	^{238}U ϵ^{int} (%)	0.330	0.383	0.375	0.436
	^{238}U ϵ^{int} (%)				
	Ring 1	0.663	0.782	0.761	0.845
	Ring 2	0.591	0.602	0.600	0.667
	Ring 3	1.047	1.089	1.167	1.194
	Ring 4	1.413	1.388	1.606	1.561
	Ring 5	0.343	0.483	0.462	0.518
	Ring 6	−3.254	−3.443	−3.646	−3.565

*The source neutron is emitted in group 56. Ring 1 is the innermost.

TABLE II

Summary of MOX One-Neutron, 281 g Source Benchmarks with the SPM*

		MOX Fuel 1 Isothermal 294 K	MOX Fuel 1 Fuel at 550 K	MOX Fuel 2 Isothermal 294 K	MOX Fuel 2 Fuel at 550 K
SUBG	ϵ^{int} (%)	1.877	2.181	2.075	2.402
	$\bar{\epsilon}$ (%)	1.928	2.110	1.919	2.096
	ϵ^{max} (%)	16.145	16.844	17.139	17.766
	In group	89	89	89	89
	^{238}U ϵ^{int} (%)	1.530	1.701	1.582	1.716
	^{239}Pu ϵ^{int} (%)	2.130	2.727	2.299	2.730
	^{240}Pu ϵ^{int} (%)	4.146	5.218	5.093	6.261
	^{241}Pu ϵ^{int} (%)	0.838	0.836	1.031	1.015
	^{241}Am ϵ^{int} (%)	2.180	2.136	2.002	1.975
	^{238}U ϵ^{int} (%)				
	Ring 1	2.481	2.808	2.490	2.772
	Ring 2	2.454	2.682	2.496	2.682
	Ring 3	1.385	1.488	1.466	1.530
	Ring 4	1.321	1.512	1.428	1.586
	Ring 5	−0.077	0.164	0.031	0.247
	Ring 6	−2.719	−3.109	−2.633	−3.036
RSE	ϵ^{int} (%)	1.795	2.036	1.981	2.244
	$\bar{\epsilon}$ (%)	2.008	2.205	1.984	2.184
	ϵ^{max} (%)	16.103	17.114	17.126	17.897
	In group	89	89	89	89
	^{238}U ϵ^{int} (%)	1.178	1.226	1.230	1.240
	^{239}Pu ϵ^{int} (%)	2.339	2.758	2.341	2.768
	^{240}Pu ϵ^{int} (%)	4.794	5.769	5.656	6.717
	^{241}Pu ϵ^{int} (%)	0.910	0.912	1.061	1.066
	^{241}Am ϵ^{int} (%)	2.229	2.205	2.048	2.043
	^{238}U ϵ^{int} (%)				
	Ring 1	2.206	2.287	2.215	2.251
	Ring 2	1.714	1.814	1.756	0.651
	Ring 3	0.600	0.697	0.680	0.737
	Ring 4	0.901	0.997	1.007	1.070
	Ring 5	0.010	0.113	0.118	0.195
	Ring 6	−2.023	−2.285	−1.938	−2.215

*The source neutron is emitted in group 56. Ring 1 is the innermost.

TABLE III

Summary of UOX One-Neutron, 295 g Source Benchmarks with the SPM*

		Case 1 Isothermal 294 K	Case 2 Reduced H_2O density	Case 3 Fuel at 900 K	Case 4 Isothermal 550 K
CALENDF	ϵ^{int} (%)	0.305	0.230	0.258	0.230
	$\bar{\epsilon}$ (%)	0.535	0.559	0.581	0.591
	ϵ^{max} (%)	5.476	5.246	6.352	5.185
	In group	79	79	91	91
	^{235}U ϵ^{int} (%)	0.071	0.076	0.158	0.107
	^{238}U ϵ^{int} (%)	0.404	0.298	0.299	0.283
	^{238}U ϵ^{int} (%)				
	Ring 1	0.829	0.696	0.839	0.622
	Ring 2	1.023	0.798	0.610	0.721
	Ring 3	0.740	0.609	0.696	0.792
	Ring 4	0.194	0.098	0.289	0.267
	Ring 5	−1.052	−0.996	−0.704	−0.867
	Ring 6	−0.895	−0.929	−1.037	−0.949
RSE	ϵ^{int} (%)	0.098	0.100	0.160	0.136
	$\bar{\epsilon}$ (%)	0.383	0.425	0.436	0.438
	ϵ^{max} (%)	3.118	3.350	5.372	4.207
	In group	114	114	91	91
	^{235}U ϵ^{int} (%)	0.175	0.163	0.200	0.174
	^{238}U ϵ^{int} (%)	0.066	0.072	0.143	0.120
	^{238}U ϵ^{int} (%)				
	Ring 1	0.015	0.088	0.177	0.133
	Ring 2	−0.220	−0.222	0.297	0.295
	Ring 3	−0.167	−0.145	0.149	−0.364
	Ring 4	0.111	0.065	0.140	−0.134
	Ring 5	0.612	0.618	0.061	0.335
	Ring 6	0.518	0.473	−0.144	0.193

*The source neutron is emitted in group 56. Ring 1 is the innermost.

TABLE IV

Summary of MOX One-Neutron, 295 g Source Benchmarks with the SPM*

		MOX Fuel 1 Isothermal 294 K	MOX Fuel 1 Fuel at 550 K	MOX Fuel 2 Isothermal 294 K	MOX Fuel 2 Fuel at 550 K
CALENDF	ϵ^{int} (%)	0.528	0.516	0.548	0.530
	$\bar{\epsilon}$ (%)	1.120	1.141	1.119	1.134
	ϵ^{max} (%)	10.443	8.616	8.925	7.344
	In group	131	131	131	131
	^{238}U ϵ^{int} (%)	0.239	0.238	0.191	0.193
	^{239}Pu ϵ^{int} (%)	0.746	0.734	0.794	0.686
	^{240}Pu ϵ^{int} (%)	1.407	1.193	1.646	1.429
	^{241}Pu ϵ^{int} (%)	0.592	0.658	0.805	0.899
	^{241}Am ϵ^{int} (%)	2.022	1.552	2.071	1.548
	^{238}U ϵ^{int} (%)				
	Ring 1	0.967	0.855	0.896	0.790
	Ring 2	1.154	1.105	1.081	1.035
	Ring 3	0.394	0.630	0.343	0.574
	Ring 4	−0.473	−0.275	−0.511	−0.317
	Ring 5	−1.972	−1.962	−1.991	−1.985
	Ring 6	−1.459	−1.291	−1.449	−1.278
RSE	ϵ^{int} (%)	0.388	0.422	0.354	0.394
	$\bar{\epsilon}$ (%)	1.006	1.067	0.979	1.037
	ϵ^{max} (%)	10.693	8.905	9.183	7.656
	In group	131	131	131	131
	^{238}U ϵ^{int} (%)	0.006	0.089	−0.011	0.060
	^{239}Pu ϵ^{int} (%)	0.631	0.663	0.595	0.631
	^{240}Pu ϵ^{int} (%)	0.826	0.718	1.246	1.115
	^{241}Pu ϵ^{int} (%)	0.805	0.808	1.054	1.076
	^{241}Am ϵ^{int} (%)	2.130	1.630	2.215	1.656
	^{238}U ϵ^{int} (%)				
	Ring 1	0.381	0.420	0.332	0.367
	Ring 2	0.100	0.697	0.059	0.651
	Ring 3	−0.559	−0.735	−0.572	−0.778
	Ring 4	−0.600	−0.753	−0.598	−0.773
	Ring 5	−0.587	−0.882	−0.560	−0.876
	Ring 6	0.234	0.081	0.286	0.112

*The source neutron is emitted in group 56. Ring 1 is the innermost.

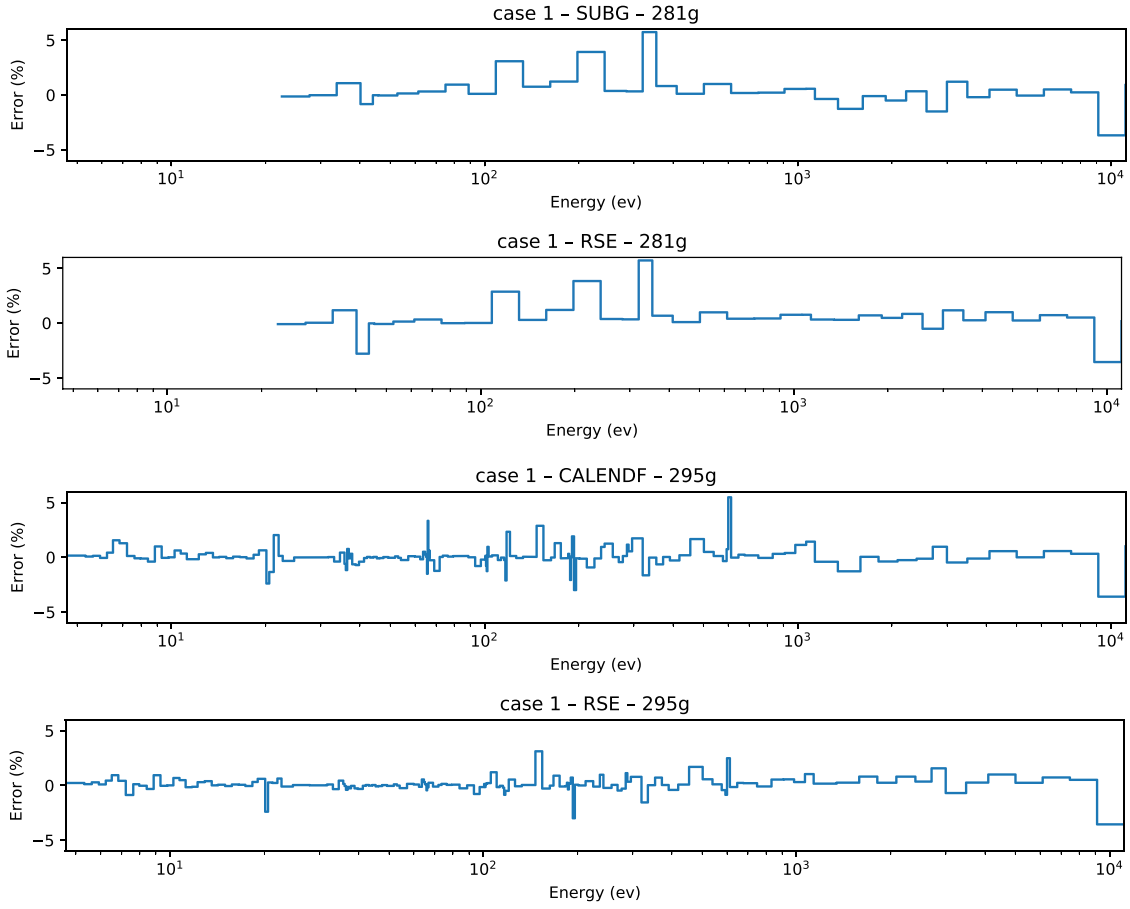

Fig. 1. UOX cases: percent error on absorption rates.

the temperatures are not those of the Rowlands benchmarks. As said before, we shifted the benchmark temperatures from 300 K to 294 K and from 600 K to 550 K in order to avoid temperature interpolation discrepancies. The GRMIN 56 option was used in the USS: module of DRAGON5. The ures option of SERPENT2 was not used. The number of source neutrons per cycle in SERPENT2 was set to 6000, the number of active cycle runs was set to 2000, and the number of inactive cycle runs was set to 20.

Tables V and VI report the values of the effective multiplication factor obtained with both the analog and implicit estimators. The discrepancies were computed with respect to the implicit estimator in SERPENT2. The numerical results show the improvement obtained by replacing the SHEM-281 with a SHEM-295 mesh and the good accuracy of the RSE self-shielding model with a SHEM-295 mesh. In all cases, the discrepancies of the effective multiplication factors obtained in the lattice calculations with RSE self-shielding were less than 70 pcm of the corresponding SERPENT2 calculations.

IV. CONCLUSION

We have proposed a reformulation of the RSE self-shielding method that can be integrated into existing subgroup implementations of lattice codes. The numerical behavior and the accuracy of the RSE method are similar to those of the subgroup method with mathematical probability tables (that is, CALENDF tables). However, the RSE tables do not suffer from the restriction of the CALENDF tables, which cannot be used with some legacy energy meshes such as the WIMS-D4, XMAS, or SHEM-281 meshes.

An open-source implementation of of the RSE method is available in version 5.0.10 of the lattice code DRAGON5.[17] Future extensions of the actual implementation will focus on the following subjects:

1. introduction of mutual resonance shielding effects
2. implementation of the resonance elastic scattering kernel model
3. introduction of spatial double-heterogeneity capabilities.

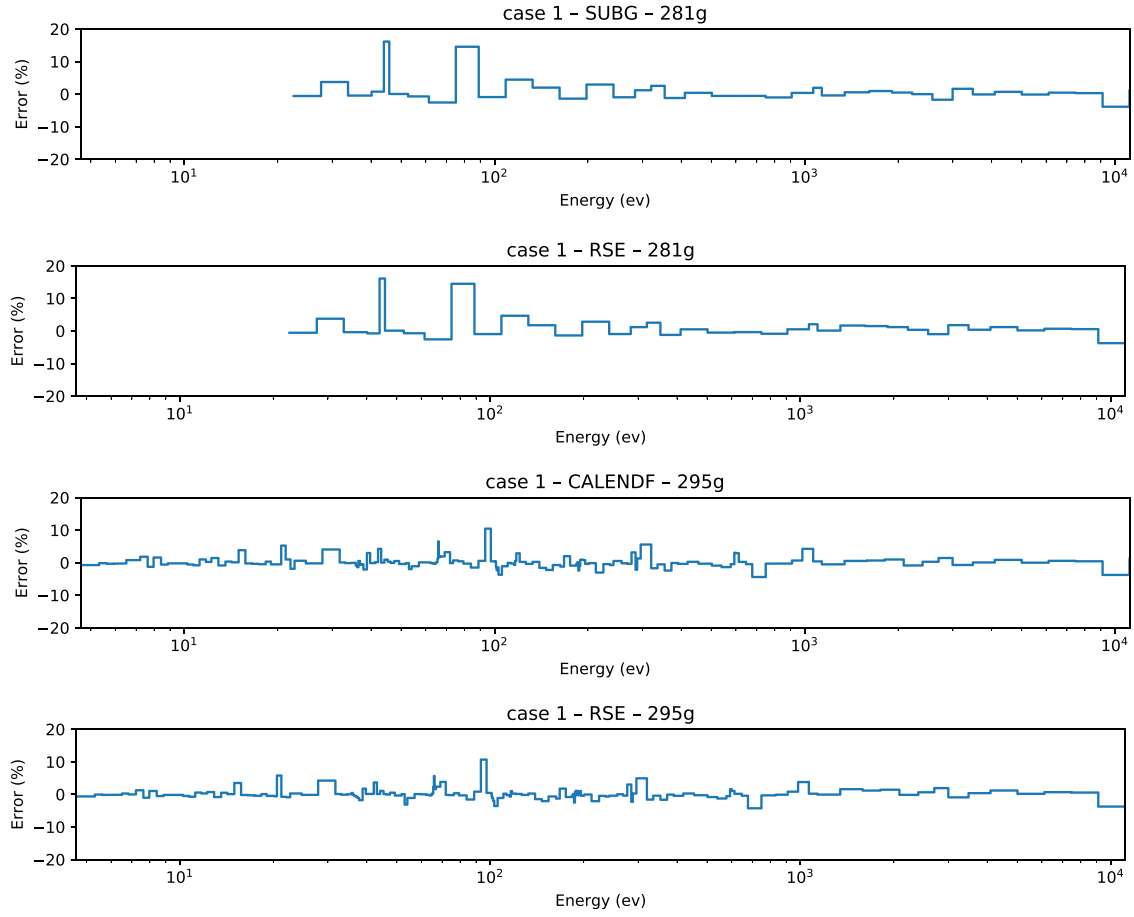

Fig. 2. MOX cases: percent error on absorption rates.

TABLE V

Summary of UOX Effective Multiplication Factors for the Rowlands 295 g Source Benchmarks*

	Case 1 Isothermal 294 K	Case 2 Reduced H_2O Density	Fuel at 900 K	Case 4 Isothermal 550 K
SERPENT2				
ANALOG IMPLICIT	1.38957 ± 37 pcm 1.38961 ± 16 pcm	1.33645 ± 38 pcm 1.33657 ± 17 pcm	1.30436 ± 36 pcm 1.30460 ± 18 pcm	1.31820 ± 37 pcm 1.31813 ± 17 pcm
DRAGON5/SHEM-281				
SUBG RSE	1.387783 (−183 pcm) 1.388371 (−124 pcm)	1.334397 (−217 pcm) 1.334895 (−168 pcm)	1.301886 (−271 pcm) 1.302746 (−185 pcm)	1.316187 (−194 pcm) 1.316950 (−118 pcm)
DRAGON5/SHEM-295				
CALENDF RSE	1.388377 (−123 pcm) 1.389115 (−50 pcm)	1.335336 (−123 pcm) 1.335895 (−68 pcm)	1.303400 (−120 pcm) 1.303762 (−37 pcm)	1.317574 (−56 pcm) 1.317944 (−19 pcm)

*The fuel is submeshed into six volumes.

TABLE VI

Summary of MOX Effective Multiplication Factors for the Rowlands 295 g Source Benchmarks*

	MOX Fuel 1 Isothermal 294 K	MOX Fuel 1 Fuel at 550 K	MOX Fuel 2 Isothermal 294 K	MOX Fuel 2 Fuel at 550 K
SERPENT2				
ANALOG IMPLICIT	1.22965 ± 42 pcm 1.22948 ± 19 pcm	1.21533 ± 42 pcm 1.21531 ± 19 pcm	1.27556 ± 43 pcm 1.27533 ± 19 pcm	1.26248 ± 44 pcm 1.26200 ± 18 pcm
DRAGON5/SHEM-281				
SUBG RSE	1.228112 (−137 pcm) 1.228176 (−130 pcm)	1.213400 (−191 pcm) 1.213706 (−160 pcm)	1.273828 (−150 pcm) 1.273936 (−139 pcm)	1.260025 (−198 pcm) 1.260384 (−162 pcm)
DRAGON5/SHEM-295				
CALENDF RSE	1.229198 (−28 pcm) 1.229652 (17 pcm)	1.214968 (−34 pcm) 1.215261 (−5 pcm)	1.275218 (−11 pcm) 1.275530 (20 pcm)	1.261858 (−14 pcm) 1.262046 (5 pcm)

*The fuel is submeshed into six volumes.

Acknowledgments

The author thanks Akio Yamamoto for helpful discussions.

Funding

This work received support from the Natural Science and Engineering Research Council of Canada under grant ALLRP 580455 - 22.

Disclosure Statement

No potential conflict of interest was reported by the author.

ORCID

Alain Hébert http://orcid.org/0000-0002-2065-1041

References

1. A. HÉBERT, *Applied Reactor Physics*, 3rd ed. Presses Internationales Polytechnique, Montréal, Quebec, Canada (2020); http://www.presses-polytechnique.ca/en/applied-reactor-physics-third-edition.
2. L. B. LEVITT, "The Probability Tables Method for Treating Unresolved Neutron Resonances in Monte-Carlo Calculations," *Nucl. Sci. Eng.*, **49**, 450 (1972); https://doi.org/10.13182/NSE72-3.
3. M. N. NIKOLAEV, "Comments on the Probability Table Method," *Nucl. Sci. Eng.*, **61**, 286 (1976); https://doi.org/10.13182/NSE61-286.
4. A. HÉBERT, "Development of the Subgroup Projection Method for Resonance Self-Shielding Calculations," *Nucl. Sci. Eng.*, **162**, 56 (2009); https://doi.org/10.13182/NSE162-56.
5. A. HÉBERT, "DRAGON5 and DONJON5, The Contribution of École Polytechnique de Montréal to the SALOME Platform," *Ann. Nucl. Energy*, **87**, 12 (2016); https://doi.org/10.1016/j.anucene.2015.02.033.
6. R. KONDO et al., "A New Resonance Calculation Method Using Energy Expansion Based on a Reduced Order Model," *Nucl. Sci. Eng.*, **195**, 694 (2021); https://doi.org/10.1080/00295639.2020.1863066.
7. H. G. LEE, C. LIM, and H. G. JO, "Improvement to the Resonance Calculation Using Energy Spectrum Expansion Method for Direct Whole-Core Calculation," presented at M&C 2023—The Int. Conf. on Mathematics and Computational Methods Applied to Nuclear Science and Engineering, Niagara Falls, Ontario, Canada (2023).
8. R. E. MACFARLANE and A. C. KAHLER, "Methods for Processing ENDF/B-VII with NJOY," *Nucl. Data Sheets*,

111, 2739 (2010); https://doi.org/10.1016/j.nds.2010.11.001.

9. A. HÉBERT, "Representation of the Temperature Correlation Effect in Lattice Calculations," *Rev. Appl. Phys.*, **3**, 18 (1994).
10. M. GRANDOTTO-BIETTOLI, "AUTOSECOL, un calcul automatique de l'auto-protection des résonances des isotopes lourds," CEA-N-1961, Commissariat à l'Énergie Atomique (1977); https://inis.iaea.org/collection/NCLCollectionStore/_Public/08/318/8318688.pdf.
11. V. SALINO and A. HÉBERT, "PyNjoy2016: An Open Source System for Producing Cross Sections Libraries for DRAGON5 and SERPENT2," presented at M&C 2023—The Int. Conf. on Mathematics and Computational Methods Applied to Nuclear Science and Engineering, Niagara Falls, Ontario, Canada (2023); https://github.com/IRSN/PyNjoy2016.
12. B. OUM-KELTOUM-AZIZA and P. RIBON, "Tables de probabilité non statistiques. Description des effets du ralentissement," presented at *PHYSOR 1990—Conf. on Physics of Reactors: Operation, Design and Computation*, Marseille, France (1990).
13. M. COSTE, "Modélisation du phénomène d'autoprotection dans le code de transport multigroupe APOLLO2," CEA-R-6114, Commissariat à l'Énergie Atomique (2006); https://inis.iaea.org/collection/NCLCollectionStore/_Public/38/027/38027626.pdf.
14. J. ROWLANDS et al., "LWR Pin Cell Benchmark Intercomparisons. An Intercomparison Study Organized by the JEF Project, with Contributions by Britain, France, Germany, The Netherlands, Slovenia and the USA," JEFF Report 25, OECD/NEA Data Bank, Organisation for Economic Co-opeartion and Development/Nuclear Energy Agency (1999); https://www.oecd-nea.org/upload/docs/application/pdf/2019-12/jefreport-15.pdf.
15. N. HFAIEDH and A. SANTAMARINA, "Determination of the Optimized SHEM Mesh for Neutron Transport Calculations," presented at M&C 2005—Mtg. of Mathematics and Computations, Supercomputing, Reactor Physics and Nuclear and Biological Applications, Avignon, France (2005).
16. V. SALINO, "JEFF-3.1.1 and JEFF-3.3 ACE Files for SERPENT2 Advanced Deposition Energy Model," IRSN/PyNjoy2016 (2023); https://github.com/IRSN/PyNjoy2016/releases/.
17. A. HÉBERT, "Dragon and Donjon: A Legacy Open-Source Reactor Physics Project at Polytechnique Montréal," presented at the Technical Mtg. on the Development and Application of Open-Source Modelling and Simulation Tools for Nuclear Reactors (ONCORE), Milano, Italy (2022).